An embedding scheme for the Dirac equation

An embedding scheme for the Dirac equation

S Crampin

Department of Physics, University of Bath, Bath BA2 7AY, UK

E-mail: s.crampin@bath.ac.uk

Abstract
An embedding scheme is developed for the Dirac Hamiltonian H. Dividing
space into regions I and II separated by surface S, an expression is derived for
the expectation value of H which makes explicit reference to a trial function
defined in I alone, with all details of region II replaced by an effective potential
acting on S and which is related to the Green function of region II. Stationary
solutions provide approximations to the eigenstates of H within I. The Green
function for the embedded Hamiltonian is equal to the Green function for the
entire system in region I. Application of the method is illustrated for the problem
of a hydrogen atom in a spherical cavity and an Au(001)/Ag/Au(001) sandwich
structure using basis sets that satisfy kinetic balance.

1. Introduction

There are many problems concerning electronic structure where attention is focused on a small
region of a larger system, at surfaces or defects in crystals being perhaps the most common. Let
us call this region I (figure 1), and the rest of the system as region II. Although not of primary
interest, region II cannot be ignored, since in general the electron wave functions in I will
be sensitive to the contents of region II. Some time ago Inglesfield [1] derived an embedding
scheme which enables the single-particle Schrödinger equation to be solved explicitly only in
region I. The influence of region II is taken into account exactly by adding an energy-dependent
non-local potential to the Hamiltonian for region I, which constrains the solutions in I to
match onto solutions in II. This embedding method has been developed into a powerful tool
most notably for surface electronic structure problems [2–5], where it has found widespread
application especially to situations where an accurate description of the spectrum of electron
states is necessary. Examples include studies of image states [6], surface states at metals
surfaces [7], static and dynamic screening [8], atomic adsorption and scattering at surfaces
[9], studies of surface optical response [10] and field emission [11]. Recent applications to
transport problems have also been described [12]. For a review of the embedding method,
see [13].

In the case of materials containing heavier elements, relativistic effects can be significant [14] and lead to important deviations from the electronic structure as predicted by the Schrödinger equation—shifts in inner core levels of 5d elements are typically several 100 or 1000 eV, valence-band shifts are on the eV scale and spin–orbit splitting is often measured in tenths of eV. Even after ignoring the concomitant changes in electron wave functions, these shifts can reorder levels and so affect calculated densities, fundamental to the determination of ground state properties within the density functional framework [15]. For this reason, most of the conventional electronic structure techniques developed for accurately solving the single-particle Schrödinger equation in solids have subsequently been modified to deal with the Dirac equation, including the relativistic augmented plane wave method [16, 17], relativistic linear muffin-tin orbital method [18], relativistic augmented spherical wave method [19] and the relativistic multiple-scattering method [20], and each has subsequently been used in studying a diverse range of problems. The last method alone has formed the basis of calculations of photoemission [21], magnetocrystalline anisotropy [22], hyperfine interactions [23] and magneto-transport [24] amongst other topics.

Inglesfield's embedding method has particular advantages that encourage its extension to the relativistic case. It permits the inclusion of extended substrates for surface and interface calculations, enables the study of isolated point defects in solids and, being a basis set technique, is highly flexible and permits full-potential studies with relative ease. At surfaces, extended substrates (as against the use of the supercell or thin-film approximation in which the crystal is approximated by a small number of layers, typically 5–7) enable the proper distinction between surface states, resonances and the continuum of bulk states [7]. The behaviour of the W(110) surface [25], where the addition of half a monolayer of Li is observed to *increase* the spin–orbit splitting of a surface state by $\sim$0.5 eV (resulting in Fermi surface crossings separated by $\sim$20% of the Brillouin zone dimension) typifies a type of problem a relativistic embedding scheme could address. Indeed, each of the topics mentioned at the end of the previous paragraph are relevant at surfaces and/or interfaces, and could be usefully investigated within a relativistic embedding framework.

In this paper we develop an embedding scheme for the Dirac equation that parallels Inglesfield's scheme for the Schrödinger equation. Inglesfield's starting point is the expectation value of the Hamiltonian using a trial wave function which is continuous in amplitude but discontinuous in derivative across the surface S separating I and II. The first-order nature of the Dirac equation precludes the use of a similar trial function. Instead, in the following section we use a trial function in which the large component is continuous and the small component discontinuous across S. Continuity in the small component is restored when the resulting equations are solved exactly. Using the Green function for region II we are able to derive an expression for the expectation value purely in terms of the trial function in I. In section 3 the application of the method is illustrated by calculating the eigenstates of a hydrogen atom within a cavity and in section 4 we determine the Green function for the embedded region. Section 5 briefly illustrates the method applied to a sandwich structure where relativistic effects are marked. We conclude with a brief summary and discussion.

2. Embedding scheme

In this section we consider region I joined onto region II (figure 1), and derive a variational principle for a trial wave function φ defined explicitly only within region I. We are primarily interested in the positive energy solutions of the Dirac equation [26], and so we refer to the upper and lower spinors of the Dirac bi-spinor solutions as the large and small components of the wave function respectively. We notionally extend φ into II as χ, an exact solution of the
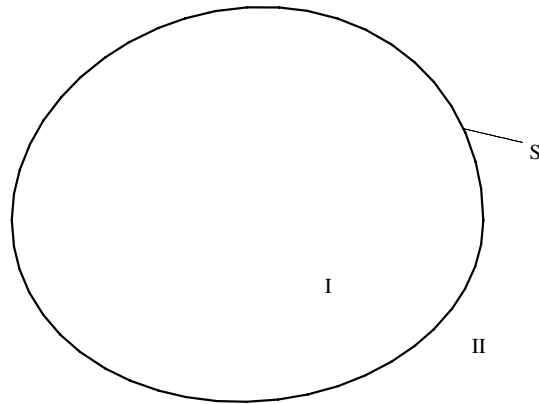
Figure 1. Schematic illustration of the embedded region I, the external region II, and the dividing surface S.

Dirac equation at some energy w, with the large components of φ and χ (φ_l and χ_l) matching on the surface S separating I and II, but with no constraint upon the small components (φ_s and χ_s), see figure 2. The expectation value for the energy W is then

$$W = \frac{\langle \varphi | \widehat{H} | \varphi \rangle_{\mathrm{I}} + \langle \chi | \widehat{H} | \chi \rangle_{\mathrm{II}} + \mathrm{i}c\hbar \int_S \mathrm{d}\boldsymbol{r}_S \cdot \varphi_l^{\dagger} \boldsymbol{\sigma} [\varphi_s - \chi_s]}{\langle \varphi | \varphi \rangle_{\mathrm{I}} + \langle \chi | \chi \rangle_{\mathrm{II}}}, \tag{1}$$

where $\widehat{H} = c\boldsymbol{\alpha}\cdot\widehat{\boldsymbol{p}} + \beta mc^2 + V$. (For clarity we omit the interaction $\propto \beta\boldsymbol{\sigma}\cdot\boldsymbol{B}$ which appears in the relativistic density functional theory [15] neglecting orbital and displacement currents, where $\boldsymbol{B}$ is a 'spin-only' effective magnetic field containing an external and exchange-correlation contribution. Its inclusion has no consequences for the derivation.) The first two terms in the numerator are the expectation value of the Hamiltonian through regions I and II, and the third the contribution due to the discontinuity in the small component of the wave function on S (in this and the following, surface normals are directed from I to II).

We eliminate reference to χ by introducing two relations. Firstly, for $\boldsymbol{r} \in \mathrm{II}$, χ satisfies the Dirac equation at energy w

$$-\mathrm{i}c\hbar\boldsymbol{\alpha} \cdot \boldsymbol{\nabla}\chi + [\beta mc^2 + V - w]\chi = 0 \tag{2}$$

and differentiating with respect to w the energy derivative of χ, $\dot{\chi} = \partial\chi/\partial w$, satisfies

$$-\mathrm{i}c\hbar\boldsymbol{\alpha} \cdot \boldsymbol{\nabla}\dot{\chi} + [\beta mc^2 + V - w]\dot{\chi} = \chi, \qquad \boldsymbol{r} \in \mathrm{II}. \tag{3}$$
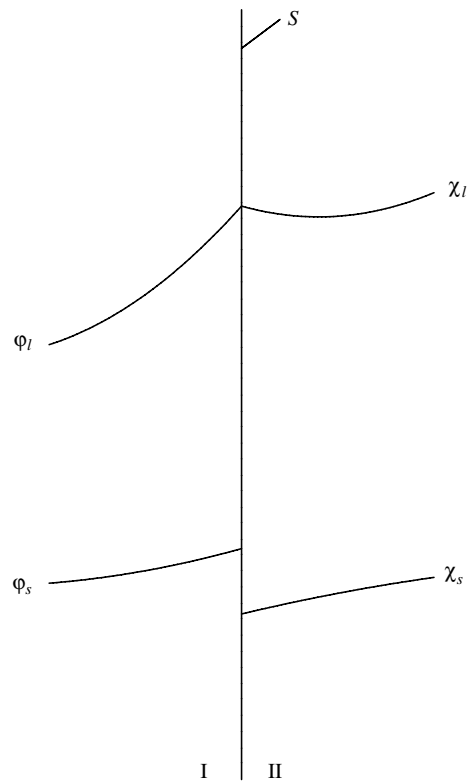
Multiplying the Hermitian conjugate of the first equation by $\dot{\chi}$ from the right, multiplying the second from the left by $\chi^{\dagger}$, subtracting and integrating over region II gives a relation between the normalization of χ in II and the amplitude on S:

$$\langle \chi | \chi \rangle_{\mathrm{II}} = \mathrm{i}c\hbar \int_S \mathrm{d}\boldsymbol{r}_S \cdot \chi_l^{\dagger} \boldsymbol{\sigma} \dot{\chi}_s. \tag{4}$$

We have assumed that χ vanishes sufficiently strongly at infinity.

For the second relation we introduce the Green function (resolvent) $G(\boldsymbol{r}, \boldsymbol{r}'; w)$ corresponding to equation (2):

$$-\mathrm{i}c\hbar\boldsymbol{\alpha} \cdot \boldsymbol{\nabla}G + [\beta mc^2 + V - w]G = -\delta(\boldsymbol{r} - \boldsymbol{r}'), \qquad \boldsymbol{r}, \boldsymbol{r}' \in \mathrm{II}. \tag{5}$$

Figure 2. The large component of the trial function is defined to be continuous across the surface *S* dividing regions I and II, but the small component can be discontinuous.

Multiplying the Hermitian conjugate of this equation by χ from the right, and subtracting $G^\dagger$ times equation (2), integrating over region II and then using the reciprocity of the Green function gives

$$\chi(r) = \mathrm{i}c\hbar \int_S \mathrm{d}r'_S \cdot G(r, r'_S; w)\boldsymbol{\alpha}\, \chi(r'_S), \qquad r \in \mathrm{II}. \tag{6}$$

We see that the Green function relates the amplitude of the wave function on *S* to the amplitude at any point within II. In particular, we can obtain a relation between the large and small components of χ on S. Writing the 4×4 Green function as

$$G(r, r'; w) = \begin{pmatrix} G_{\mathrm{ll}}(r, r'; w) & G_{\mathrm{ls}}(r, r'; w) \\ G_{\mathrm{sl}}(r, r'; w) & G_{\mathrm{ss}}(r, r'; w) \end{pmatrix}, \tag{7}$$

where each entry is a 2×2 matrix, substituting into equation (6), and rearranging the two equations coupling the small and large components of χ gives

$$\chi_{\mathrm{s}}(r_S) = \mathrm{i}c\hbar \int_S \mathrm{d}r'_S \cdot \Gamma(r_S, r'_S; w)\boldsymbol{\sigma}\, \chi_{\mathrm{l}}(r'_S), \tag{8}$$

where

$$\Gamma(r_S, r'_S; w) = G_{\mathrm{ss}}(r_S, r'_S; w) + \mathrm{i}c\hbar \int_S \mathrm{d}r''_S \cdot G_{\mathrm{sl}}(r_S, r''_S; w)\boldsymbol{\sigma}\, \Gamma(r''_S, r'_S; w). \tag{9}$$

It follows from (6) that the Green functions in (9) are the limiting forms of $G(r, r_S; w)$ as $r \to r_S$ from within II.

Equations (4) and (8) are the desired results that enable us to express the expectation value W in (1) in terms of φ alone. After substitution and use of the continuity of the large components $\chi_l = \varphi_l$ on S we obtain

$$W = \frac{\langle \varphi | \widehat{H} | \varphi \rangle_{\mathrm{I}} + \mathrm{i}c\hbar \int_S \mathrm{d}r_S \cdot \varphi_l^{\dagger} \boldsymbol{\sigma} [\varphi_s - \mathrm{i}c\hbar \int_S \mathrm{d}r_S' \cdot \{\Gamma - w\dot{\Gamma}\} \boldsymbol{\sigma} \varphi_l]}{\langle \varphi | \varphi \rangle_{\mathrm{I}} - c^2\hbar^2 \int_S \mathrm{d}r_S \cdot \varphi_l^{\dagger} \boldsymbol{\sigma} \int_S \mathrm{d}r_S' \cdot \dot{\Gamma} \boldsymbol{\sigma} \varphi_l}. \tag{10}$$

This is an expression for the expectation value of the energy W, given purely in terms of the trial function φ in region I and on the surface S, with all details of region II entering via Γ and its energy derivative. Following the convention in the non-relativistic embedding scheme we shall refer to Γ as the embedding potential.

To see what this variational principle means in practice, we consider variations in $\varphi^{\dagger}$, whereby

$$\delta W = \frac{\langle \delta\varphi | \widehat{H} - W | \varphi \rangle_{\mathrm{I}} + \mathrm{i}c\hbar \int_S \mathrm{d}r_S \cdot \delta\varphi_l^{\dagger} \boldsymbol{\sigma} [\varphi_s - \mathrm{i}c\hbar \int_S \mathrm{d}r_S' \cdot \{\Gamma + (W - w)\dot{\Gamma}\} \boldsymbol{\sigma} \varphi_l]}{\langle \varphi | \varphi \rangle_{\mathrm{I}} - c^2\hbar^2 \int_S \mathrm{d}r_S \cdot \varphi_l^{\dagger} \boldsymbol{\sigma} \int_S \mathrm{d}r_S' \cdot \dot{\Gamma} \boldsymbol{\sigma} \varphi_l}, \tag{11}$$

so that solutions φ stationary with respect to arbitrary variations $\delta\varphi$ satisfy

$$\widehat{H}\varphi = W\varphi, \qquad r \in \mathrm{I}, \tag{12a}$$

$$\varphi_s(r_S) = \mathrm{i}c\hbar \int_S \mathrm{d}r_S' \cdot \{\Gamma(r_S, r_S'; w) + (W - w)\dot{\Gamma}(r_S, r_S'; w)\} \boldsymbol{\sigma} \varphi_l(r_S'). \tag{12b}$$

The first expression indicates φ is a solution of the Dirac equation at energy W in region I. Comparing the second with (8) shows that φ also possesses the correct relationship between large and small components on S, the surface separating I and II, to match onto solutions in II. The term $(W - w)\dot{\Gamma}(w)$ provides a first-order correction to $\Gamma(w)$ so that the boundary condition is appropriate for energy W.

In practice, expression (10) may be used to obtain solutions of the Dirac Hamiltonian by inserting a suitably parametrized trial function and varying the parameters to obtain a stationary solution. This is conveniently achieved by expanding the trial solution in a finite basis of separate large and small component spinors

$$\varphi(r) = \sum_{n=1}^{N_l} a_{l,n} \begin{bmatrix} \psi_{l,n}(r) \\ 0 \end{bmatrix} + \sum_{n=1}^{N_s} a_{s,n} \begin{bmatrix} 0 \\ \psi_{s,n}(r) \end{bmatrix} = \begin{bmatrix} \boldsymbol{\psi}_l(r) & 0 \\ 0 & \boldsymbol{\psi}_s(r) \end{bmatrix} \begin{bmatrix} a_l \\ a_s \end{bmatrix}. \tag{13}$$

The matrix in the final expression is $4 \times (N_l + N_s)$, and the column vector contains the $N_l + N_s$ coefficients. Substituting into (10) we find states ϕ that are stationary with respect to variations in the expansion coefficients $\{a_{l,n}, a_{s,n}\}$ are then given by the eigenstates of a generalized eigenvalue problem of the form

$$\begin{bmatrix} H_{ll} & H_{ls} \\ H_{sl} & H_{ss} \end{bmatrix} \begin{bmatrix} a_l \\ a_s \end{bmatrix} = W \begin{bmatrix} O_{ll} & 0 \\ 0 & O_{ss} \end{bmatrix} \begin{bmatrix} a_l \\ a_s \end{bmatrix}, \tag{14}$$

where

$$[H_{\text{ll}}]_{nn'} = \int_I \psi_{1,n}^\dagger(\boldsymbol{r})(V(\boldsymbol{r}) + mc^2)\psi_{1,n'}(\boldsymbol{r})\,\mathrm{d}\boldsymbol{r}$$

$$+ c^2\hbar^2 \int_S \mathrm{d}\boldsymbol{r}_S \cdot \psi_{1,n}^\dagger(\boldsymbol{r}_S)\boldsymbol{\sigma} \int_S \mathrm{d}\boldsymbol{r}_S' \cdot [\Gamma(\boldsymbol{r}_S, \boldsymbol{r}_S'; w) - w\dot\Gamma(\boldsymbol{r}_S, \boldsymbol{r}_S'; w)]\boldsymbol{\sigma}\psi_{1,n'}(\boldsymbol{r}_S'), \quad (15a)$$

$$[H_{\text{ls}}]_{nn'} = \int_I \psi_{1,n}^\dagger(\boldsymbol{r})c\boldsymbol{\sigma} \cdot \widehat{\boldsymbol{p}}\psi_{s,n'}(\boldsymbol{r})\,\mathrm{d}\boldsymbol{r} + \mathrm{i}c\hbar \int_S \mathrm{d}\boldsymbol{r}_S \cdot \psi_{1,n}^\dagger(\boldsymbol{r}_S)\boldsymbol{\sigma}\psi_{s,n'}(\boldsymbol{r}_S), \quad (15b)$$

$$[H_{\text{sl}}]_{nn'} = \int_I \psi_{s,n}^\dagger(\boldsymbol{r})c\boldsymbol{\sigma} \cdot \widehat{\boldsymbol{p}}\psi_{1,n'}(\boldsymbol{r})\,\mathrm{d}\boldsymbol{r}, \quad (15c)$$

$$[H_{\text{ss}}]_{nn'} = \int_I \psi_{s,n}^\dagger(\boldsymbol{r})(V(\boldsymbol{r}) - mc^2)\psi_{s,n'}(\boldsymbol{r})\,\mathrm{d}\boldsymbol{r}, \quad (15d)$$

$$[O_{\text{ll}}]_{nn'} = \int_I \psi_{1,n}^\dagger(\boldsymbol{r})\psi_{s,n'}(\boldsymbol{r})\,\mathrm{d}\boldsymbol{r} - c^2\hbar^2 \int_S \mathrm{d}\boldsymbol{r}_S \cdot \psi_{1,n}^\dagger(\boldsymbol{r}_S)\boldsymbol{\sigma} \int_S \mathrm{d}\boldsymbol{r}_S' \cdot \dot\Gamma(\boldsymbol{r}_S, \boldsymbol{r}_S'; w)\boldsymbol{\sigma}\psi_{1,n'}(\boldsymbol{r}_S'),$$

$$(15e)$$

$$[O_{\text{ss}}]_{nn'} = \int_I \psi_{s,n}^\dagger(\boldsymbol{r})\psi_{s,n'}(\boldsymbol{r})\,\mathrm{d}\boldsymbol{r}. \quad (15f)$$

Of course, the spectrum of the Dirac Hamiltonian is unbounded below, and care must be taken to prevent solutions collapsing to negative energies. This can be avoided through the use of a kinetically balanced basis [27] in which there is a one-to-one relationship between large and small component spinors, $N_s = N_1 = N$, and where the small component spinors are given by

$$\psi_{s,n}(\boldsymbol{r}) = \boldsymbol{\sigma} \cdot \widehat{\boldsymbol{p}}\psi_{1,n}(\boldsymbol{r}). \quad (16)$$

The upper half of the spectrum of the $2N$ eigenstates of (14) then provide approximations to the spectrum of electronic states.

3. Model application

To illustrate the application of the relativistic embedding scheme we consider a model problem of a hydrogen atom within a spherical cavity, finding bound states of the Dirac equation corresponding to the potential illustrated in figure 3:

$$V(\boldsymbol{r}) = \begin{cases} -\lambda/r, & r \leqslant R, \\ V_0, & r > R, \end{cases}$$

where $\lambda = e^2/(4\pi\epsilon_0)$ and $V_0 > 0$. We choose this model as the bound states may also be found straightforwardly by alternative methods. Region I, the region to be treated explicitly, is the sphere of radius R centred on $r = 0$. The external region II where $V(r) = V_0$ is replaced by an embedding potential acting on the surface of the sphere. The value of the embedding potential is most readily evaluated from equation (8). A general solution to the Dirac equation at some energy w in region II and satisfying the appropriate boundary conditions is [26]

$$\chi(\boldsymbol{r}) = \begin{pmatrix} \chi_1(\boldsymbol{r}) \\ \chi_s(\boldsymbol{r}) \end{pmatrix} = \sum_\Lambda a_\Lambda \sqrt{\frac{\pi}{2kr}} \begin{pmatrix} K_{\ell+\frac{1}{2}}(kr)\Omega_\Lambda(\boldsymbol{r}) \\ -\mathrm{i}\gamma_\kappa K_{\bar\ell+\frac{1}{2}}(kr)\Omega_{\bar\Lambda}(\boldsymbol{r}) \end{pmatrix}, \quad (17)$$

where $\Lambda = (\kappa, \mu)$, $\bar\Lambda = (-\kappa, \mu)$, $\Omega_\Lambda(\boldsymbol{r})$ a spin-angular function, $K_{n+\frac{1}{2}}(z)$ a modified spherical Bessel function of the third kind [28], $c\hbar k = \sqrt{m^2c^4 - (w - V_0)^2}$, $\gamma_\kappa = \hbar ck/(w - V_0 + mc^2)$ and

$$\ell = \begin{cases} \kappa, & \kappa > 0, \\ -(\kappa + 1), & \kappa < 0, \end{cases} \qquad \bar\ell = \ell - \frac{\kappa}{|\kappa|}. \quad (18)$$
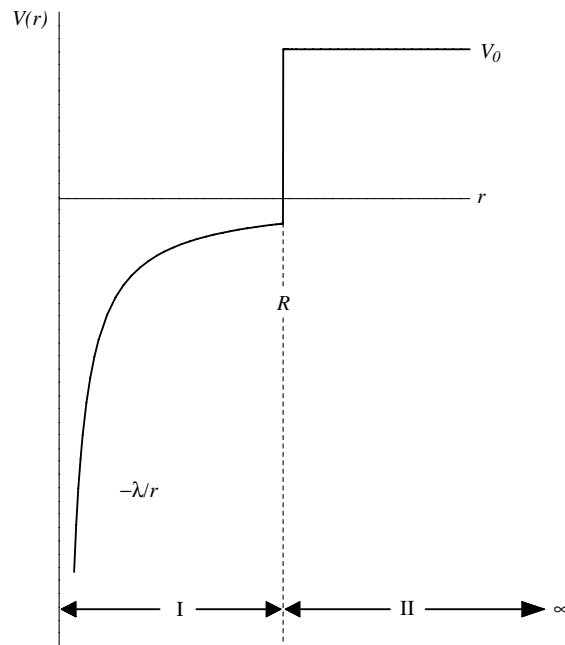
Figure 3. The model potential used to illustrate the relativistic embedding scheme.

The spherical symmetry of region II means the the embedding potential Γ may be expanded on S as

$$\Gamma(r_S, r'_S; w) = \sum_{\Lambda} \Gamma_{\kappa}(w)\Omega_{\bar{\Lambda}}(r_S)\omega_{\bar{\Lambda}}^{\dagger}(r'_S) \tag{19}$$

and substituting (19) and (17) into (8) leads to

$$\Gamma_{\kappa}(w) = \frac{\gamma_{\kappa}}{c\hbar R^2} \frac{K_{\bar{\ell}+\frac{1}{2}}(kR)}{K_{\ell+\frac{1}{2}}(kR)}. \tag{20}$$

Using (9) with the Green function for constant potential ($w < V_0, r > r'$)

$$G(r, r'; w) = -\frac{(w - V_0 + mc^2)}{c^2\hbar^2 r} \sum_{\Lambda} \begin{pmatrix} K_{\ell+\frac{1}{2}}(kr)\Omega_{\Lambda}(r) \\ -i\gamma_{\kappa}K_{\bar{\ell}+\frac{1}{2}}(kr)\Omega_{\bar{\Lambda}}(r) \end{pmatrix} \begin{pmatrix} I_{\ell+\frac{1}{2}}(kr')\Omega_{\Lambda}(r') \\ i\gamma_{\kappa}I_{\bar{\ell}+\frac{1}{2}}(kr')\Omega_{\bar{\Lambda}}(r') \end{pmatrix}^{\dagger} \tag{21}$$

gives the same result but, rather, after more involved manipulations. $I_{n+\frac{1}{2}}(z)$ is a modified spherical Bessel function of the first kind.

Because of the spherical symmetry we can determine separately states with a given angular character Λ. Using as a basis set for the large component spinors

$$\psi_{1,n}^{(\Lambda)}(r) = \frac{1}{r}g_n(r)\Omega_{\Lambda}(r), \qquad g_n(r) = r^n e^{-r} \tag{22}$$

so that the small component spinors ensuring kinetic balance are

$$\psi_{s,n}^{(\Lambda)}(r) = \frac{i}{r}f_{n\kappa}(r)\Omega_{\bar{\Lambda}}(r), \qquad f_{n\kappa}(r) = \hbar[(n+\kappa)r^{n-1} - r^n]e^{-r}, \tag{23}$$

Table 1. Lowest two electron-like eigenvalues $E = W - mc^2$ of $s_{1/2}$ symmetry of a hydrogen atom confined to a spherical cavity with radius $R = 3$ and confining potential $V = 10$, obtained by using embedding potentials at different trial energies w. $w = W$ indicates the solution has been iterated to ensure that w coincides with the eigenvalue. The exact eigenvalues are those found by matching internal and external solutions at R. We use atomic units $e^2 = \hbar = m = 1$ and $c = 137.035\,999\,76$ so that the corresponding free atom eigenvalues are $-0.500\,0067$ and $-0.125\,0021$.

N_l	$w = mc^2 - 0.5$	$w = mc^2$	$w = W$
2	$-0.411\,1620$, $1.698\,0995$	$-0.411\,1527$, $1.694\,9300$	$-0.411\,1624$, $1.689\,6482$
4	$-0.445\,1482$, $0.912\,9418$	$-0.445\,1439$, $0.912\,6817$	$-0.439\,6204$, $0.971\,4775$
6	$-0.445\,5519$, $0.891\,4789$	$-0.445\,5477$, $0.891\,2219$	$-0.445\,5520$, $0.891\,0268$
8	$-0.445\,5532$, $0.891\,2708$	$-0.445\,5488$, $0.891\,0141$	$-0.445\,5532$, $0.890\,8194$
'Exact'	$-0.445\,5532$, $0.890\,8194$	$-0.445\,5532$, $0.890\,8194$	$-0.445\,5532$, $0.890\,8194$

the matrix elements become

$$[H_{ll}^{(\Lambda)}]_{nn'} = \int_0^R g_n(r) \left[-\frac{\lambda}{r} + mc^2 \right] g_{n'}(r)\, dr + \hbar^2 c^2 R^2 g_n(R) g_{n'}(R) [\Gamma_\kappa(w) - w \dot{\Gamma}_\kappa(w)],$$

(24a)

$$[H_{ss}^{(\Lambda)}]_{nn'} = \int_0^R f_{n\kappa}(r) \left[-\frac{\lambda}{r} - mc^2 \right] f_{n'\kappa}(r)\, dr,$$

(24b)

$$[H_{ls}^{(\Lambda)}]_{nn'} = -\hbar c \int_0^R g_n(r) \left[\frac{d f_{n'\kappa}(r)}{dr} - \frac{\kappa}{r} f_{n'\kappa}(r) \right] dr + \hbar c g_n(R) f_{n'\kappa}(R),$$

(24c)

$$[H_{sl}^{(\Lambda)}]_{nn'} = \hbar c \int_0^R f_{n\kappa}(r) \left[\frac{dg_{n'}(r)}{dr} + \frac{\kappa}{r} g_{n'}(r) \right] dr,$$

(24d)

$$[O_{ll}^{(\Lambda)}]_{nn'} = \int_0^R g_n(r) g_{n'}(r)\, dr - \hbar^2 c^2 R^2 g_n(R) g_{n'}(R) \dot{\Gamma}_\kappa(w),$$

(24e)

$$[O_{ss}^{(\Lambda)}]_{nn'} = \int_0^R f_{n\kappa}(r) f_{n'\kappa}(r)\, dr.$$

(24f)

The eigenvalues only depend upon the quantum number κ. In table 1 the two lowest eigenvalues of $\kappa = -1$ symmetry (corresponding to the $1s_{1/2}$ and $2s_{1/2}$ of free hydrogen) are shown as a function of the basis set size and for different values of the energy w at which the embedding potential is evaluated, for the case $R = 3$, $V_0 = 10$. For comparison also given are the values found by matching the external solution (17) to the regular internal solution, which can be expressed in terms of confluent hypergeometric functions [26]. For a given fixed w, the eigenvalues converge from above to values that are equal to or above the exact values. The further w lies from the eigenvalue, the larger the difference between the limiting value for large basis sets and the correct value. However, the influence of the $\dot{\Gamma}$ terms in (10) means the error is relatively small. When $w = mc^2$, the lowest eigenvalue found with $N_l = 8$ is $-0.445\,5488$ Ha and in error by only $0.000\,0044$ Ha, a factor 10^5 smaller than the error in w.

Differentiating (10) with respect to the trial energy w shows the expectation value is stationary at $w = W$. In this case, W is given by the solutions of

$$W = \frac{\langle \varphi | \widehat{H} | \varphi \rangle_I + \mathrm{i} c\hbar \int_S dr_S \cdot \varphi_l^\dagger \boldsymbol{\sigma} \left[\varphi_s - \mathrm{i} c\hbar \int_S dr_S' \cdot \Gamma(W) \boldsymbol{\sigma} \varphi_l \right]}{\langle \varphi | \varphi \rangle_I}.$$

(25)

Eigenfunctions φ solving this equation satisfy the Dirac equation within region I and the relationship between the small and large components on S (12b) is exact. The final column in table 1 shows the two lowest positive energy eigenvalues of (25), again as a function of basis set size. The eigenvalues again converge from above, and by $N_l = 8$ reproduce the exact values by at least seven significant figures. It is worth noting that with this particular basis set, increasing N_l much further leads to some numerical difficulties due to overcompleteness. For more accurate work, a more suitable basis set should be used. It should also be noted that conventional finite basis set calculations using a basis satisfying kinetic balance can give eigenvalues that lie below exact limiting values by an amount of order $1/c^4$ [27], and a similar behaviour is expected in this embedding scheme.

4. Green function

Most practical applications of the Schrödinger embedding scheme have actually used the Green function of the embedded system. This is a more convenient quantity when dealing with systems where the spectrum is continuous, such as at surfaces or defects in solids. We therefore consider the Green function for the embedded Dirac system.

Differentiating (10) with respect to w shows W is stationary when $w = W$, as would be expected. In this case stationary solutions satisfy the embedded Dirac equation

$$\widehat{H}\varphi(r) + \int_I dr' \Delta(r, r'; W)\varphi(r') - W\varphi(r) = 0, \qquad r \in I, \tag{26}$$

where, introducing $\sigma_S(r_S)$, the component of σ in the direction normal to the surface S (from I to II) at r_S, the additional term Δ enforcing the embedding is

$$\Delta(r, r'; w) = \int_S dr_S \delta(r - r_S) \int_S dr'_S \, \delta(r' - r'_S)$$
$$\times \begin{bmatrix} c^2\hbar^2\sigma_S(r_S)\Gamma(r_S, r'_S; w)\sigma_S(r'_S) & ic\hbar\sigma_S(r_S)\delta(r_S - r'_S) \\ 0 & 0 \end{bmatrix}. \tag{27}$$

The corresponding Green function satisfies

$$\widehat{H}G(r, r'; W) + \int_I dr'' \, \Delta(r, r''; W)G(r'', r'; W) - WG(r, r'; W) = -\delta(r - r') \tag{28}$$

for $r, r' \in I$. A line of argument similar to that given by Inglesfield [1] for the embedded Schrödinger equation shows that this Green function is identical for $r, r' \in I$ to the Green functions G_{I+II} for the entire system I+II. For simplicity, assuming that I+II constitutes a finite system so that the spectrum is discrete, the Green function G_{I+II} is given by

$$G_{I+II}(r, r'; W) = \sum_n \frac{\Psi_n(r)\Psi_n^\dagger(r')}{W - W_n^{I+II}}, \tag{29}$$

where W_n^{I+II} is the eigenvalue corresponding to eigenstate $\Psi_n(r)$ of the entire system, normalized to unity over I+II. For a given W, the Green function obtained by solving (28) can be expanded in terms of the eigenstates $\varphi_n(r; W)$ of the corresponding homogeneous equation

$$\widehat{H}\varphi_n(r; W) + \int_I dr' \, \Delta(r, r'; W)\varphi_n(r'; W) - W_n(W)\varphi_n(r; W) = 0, \qquad r \in I \tag{30}$$

normalized to unity over I, as

$$G(r, r'; W) = \sum_n \frac{\varphi_n(r; W)\varphi_n^\dagger(r'; W)}{W - W_n(W)}. \tag{31}$$

Clearly, G has poles at $W = W_n(W)$. At these energies (30) and becomes the exact embedded Dirac equation (26) and as we have seen the poles will occur at eigenstates of the entire system and the spectrum of G and G_{I+II} coincide. It remains to show the poles of G have the appropriate weight. The residue of G at W_n is

$$\frac{\varphi_n(r; W_n)\varphi_n^\dagger(r'; W_n)}{1 - (\partial W_n(W)\partial W)|_{W_n}} = \frac{\varphi_n(r; W_n)\varphi_n^\dagger(r'; W_n)}{1 - c^2\hbar^2 \int_S dr_S \cdot \varphi_l^\dagger \boldsymbol{\sigma} \int_S dr_S' \cdot \dot{\Gamma}(W_n)\boldsymbol{\sigma}\varphi_l}. \tag{32}$$

The second term in the denominator is precisely the additional factor necessary to correctly normalize the states (see (4), (8)) so that

$$\frac{\varphi_n(r; W_n)\varphi_n^\dagger(r'; W_n)}{1 - (\partial W_n(W)/\partial W)|_{W_n}} = \Psi_n^\dagger(r)\Psi_n(r'). \tag{33}$$

The residues of the Green function of the embedded system and those of the entire system are identical. Hence the two Green functions are identical for $r, r' \in I$.

For practical calculations the Green function can be expanded using a double-basis of separate large and small component spinors:

$$G(r, r'; W) = \begin{bmatrix} \boldsymbol{\psi}_l(r) & 0 \\ 0 & \boldsymbol{\psi}_s(r) \end{bmatrix} G(W) \begin{bmatrix} \boldsymbol{\psi}_l(r') & 0 \\ 0 & \boldsymbol{\psi}_s(r') \end{bmatrix}^\dagger. \tag{34}$$

The elements of the matrix of coefficients G may be found by substituting into (28), multiplying from the right by the vector of basis functions, multiplying from the left by the Hermitian transpose of the vector of basis functions, and integrating over region I. This leads to

$$G(W) = \begin{bmatrix} WO_{ll} - H_{ll} & -H_{ls} \\ -H_{sl} & WO_{ss} - H_{ss} \end{bmatrix}^{-1}, \tag{35}$$

where the overlap and Hamiltonian matrices have their previous definitions (15a)–(15f) with $\dot{\Gamma} = 0$.

As an illustration we calculate the local density of states for the confined hydrogen model at energies above V_0 where the spectrum is continuous. Integrating over the embedded region this is given by

$$n(W) = -\frac{1}{\pi} \operatorname{Im} \operatorname{Tr} G(W + i0^+)O. \tag{36}$$

Figure 4 shows the $s_{1/2}$ wave local density of states for $R = 3$, $V = 1$, calculated with varying number of basis functions. The basis functions (22), (23) are not particularly appropriate for representing the continuum wave solutions, and so convergence is only achieved using a relatively large set; however the results serve to illustrate the systematic improvement that accompanies an increasing number of basis functions. The local density of states shows two resonances, the precursors of bound states that exist when any of R, Z or V_0 are increased sufficiently.

5. Application to an embedded monolayer

As a further example, one that provides a test of the relativistic embedding scheme when applied to a more challenging problem, we use it to calculate the local density of states on a silver monolayer in a Au(001)/Ag/Au(001) sandwich structure. Using the embedding scheme only the region occupied by the Ag monolayer is explicitly treated. This is region I, with the two Au halfspaces on either side entering the calculation via embedding potentials expanded on planar surfaces. Then, using Bloch's theorem the calculation is performed within a unit
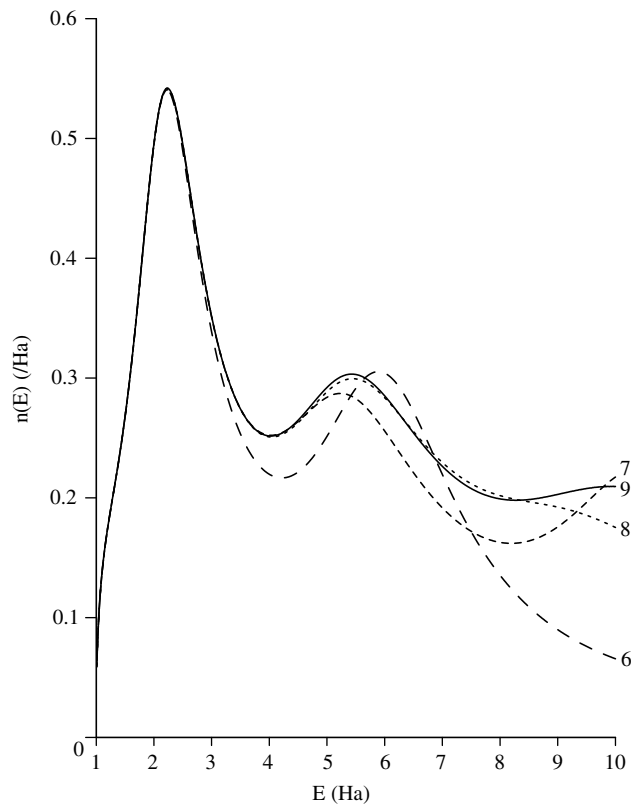
Figure 4. The $s_{1/2}$-wave local density of states as a function of energy $E = W - mc^2$, integrated through a sphere of radius $R = 3$ for the model system of a confined hydrogen atom with model parameters $R = 3$, $V_0 = 1$. Different curves have been calculated with basis sets corresponding to the indicated number N_l of basis functions.

cell containing one atom. The full technical details will be described elsewhere, but briefly the Green function at two-dimensional wave vector K is expanded in a set of linearized augmented relativistic plane waves. We use large component basis functions

$$\psi_{l,G\sigma}(r) = \begin{cases} \varphi_\sigma \exp(i(K + G) \cdot r), & r \in \text{interstitial}, \\ \sum_\Lambda \left[A_\kappa^{G\sigma} u_\kappa(r) + B_\kappa^{G\sigma} \dot{u}_\kappa(r), \right] \Omega_\Lambda(\widehat{r}) & r \in \text{muffin-tin}, \end{cases} \quad (37)$$

where φ_σ is a Pauli spinor, $G = g + G_z \hat{z}$, with g a two-dimensional reciprocal lattice vector and $G_z = n \times 2\pi/\tilde{D}$, $n = 0, \pm 1, \pm 2, \dots$ and where $\tilde{D}$ exceeds the width of the embedded region ensuring variational freedom in the basis. The function u_κ is the large component of the wavefunction that satisfies the radial Dirac equation for the spherically symmetric component of the potential at some pivot energy; $\dot{u}_\kappa$ is the energy derivative of u_κ. The matching coefficients A_κ^G, B_κ^G ensure continuity of the basis function in amplitude and derivative at the muffin-tin radius. The small component basis functions are chosen to satisfy kinetic balance.

Overlap and Hamiltonian matrix elements follow directly from these basis functions. The embedding potential is obtained from (8) using the general expression for a wavefunction outside a surface at wave vector K. This gives for the embedding potential describing the left
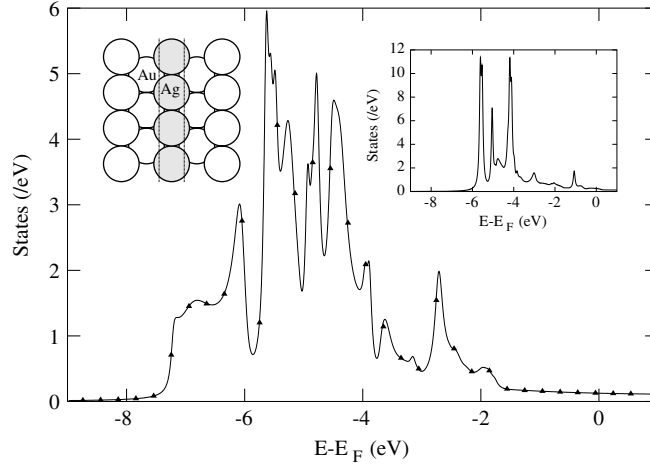
Figure 5. Local density of states on a Ag monolayer in a Au(001)/Ag/Au(001) sandwich structure calculated using a relativistic scattering method (——) and relativistic embedding (▲). The insets show the calculation geometry (left) and the local density of states obtained from the Schrödinger equation (right).

Au half space

$$\Gamma(\boldsymbol{r}_S, \boldsymbol{r}'_S) = \frac{\mathrm{i}}{W + mc^2} \sum_{g\sigma g'\sigma'} [(S^- + S^+ R^{+-})(1 + R^{+-})^{-1}\sigma_z]_{g\sigma g'\sigma'}$$

$$\times \exp(\mathrm{i}(\boldsymbol{K} + \boldsymbol{g}) \cdot \boldsymbol{r}_S) \exp(-\mathrm{i}(\boldsymbol{K} + \boldsymbol{g}') \cdot \boldsymbol{r}'_S)\varphi_\sigma \otimes \varphi_{\sigma'} \quad (38)$$

with

$$S^{\pm}_{g\sigma g'\sigma'} = \varphi^\dagger_\sigma \left(\boldsymbol{\sigma} \cdot \boldsymbol{K}^{\pm}_g\right) \varphi_{\sigma'} \delta_{gg'}. \quad (39)$$

The reflection matrix $R^{\pm}$ is found using standard layer-scattering methods [29]. A similar approach may be used to obtain an embedding potential for the right half space, which unlike the non-relativistic case differs from that for the left half space.

Figure 5 compares the local density of states calculated using the relativistic embedding technique for an embedded Ag monolayer using embedding potentials corresponding to Au(001) with that found for an Au(001)/Ag/Au(001) sandwich geometry using relativistic scattering theory [29]. The same Au and Ag potentials have been used in each case, and the local density of states found within the same muffin-tin volume. Therefore the results obtained with the two methods should be comparable, and we find that they are indistinguishable. This confirms that the embedding potential (38) imposes the correct variational constraint upon wave functions for the embedded Ag monolayer so that they replicate the behaviour of an extended Au(001)/Ag/Au(001) sandwich structure. The inset in figure 5 shows the local density of states in the non-relativistic limit ($c \longrightarrow \infty$), indicating the significant relativistic effects on the electronic structure which are correctly reproduced with this Dirac-embedding scheme.

6. Summary and discussion

We have outlined above an embedding scheme for the Dirac equation. It enables the Dirac equation to be solved within a limited region I when this region forms part of a larger system,

I + II. Region II is replaced by an additional term added to the Hamiltonian for region I, and which acts on the surface S separating I and II. The embedding scheme is derived using a trial function in which continuity in the small component across S is imposed variationally. Expanding the wave function in a basis set of separate large and small component spinors, the problem of variational collapse is avoided by using a basis satisfying kinetic balance. Calculating the spectrum of a confined hydrogen atom, the method is shown to be stable and converge to the exact eigenvalues. We have also derived the Green function for the embedded Hamiltonian and illustrated its use in the continuum regime of the same confined hydrogen system and an Au/Ag/Au sandwich structure. These are demonstration calculations—future applications are likely to be to defects and surfaces of materials containing heavier (typically 5d) elements, within the framework of density functional theory.

It is worthwhile to discuss further the use of a trial function that is discontinuous in the small component, since such a wave function gives rise to a discontinuous probability density and so would normally be dismissed in quantum theory. In non-relativistic quantum mechanics discontinuous trial functions are not permitted, since they possess infinite energy. However, the Dirac equation is first order in p and as we have seen a perfectly regular expectation value of H results. Exploiting this freedom, the embedding scheme outlined above leads to solutions that are continuous in both large and small component *only* when the embedding potential $\Gamma(r_S, r'_S; w)$ is evaluated at the same energy w as the energy W that appears in the Dirac equation itself, for then the relationship between small and large components on S inside (equation (12b)) and outside (equation (8)) coincide, the large components matching by construction. This may be achieved for example via the iterative scheme used in connection with equation (25) and the final column of table 1, or explicitly when determining the Green function as in section 4. These are the methods in which the non-relativistic embedding scheme has been most widely used.

When w and W do not coincide, the solutions obtained via this embedding scheme will retain small components that are discontinuous across S. This may be unacceptable for certain applications, but the solutions continue to be valid approximations at least in as much as they provide estimates of the energies of the solutions of the Dirac equation, and so could suffice, e.g. for interpreting spectroscopic measurements. This embedding scheme places no greater emphasis on a discontinuity in the small amplitude at S than on an incorrect (but continuous) amplitude elsewhere within the embedded region. It aims merely to optimize the energy of the state, and will retain a discontinuity in the small component if in doing so it can better (in terms of energy) approximate the solution inside the embedded region. In the non-relativistic embedding scheme, the discontinuous derivative of the trial function implies a probability current (and electric current) that is discontinuous across the embedding surface. This is similarly unphysical, yet numerous applications such as those cited above have demonstrated the utility and accuracy of the method. Indeed, there have been many applications in which this scheme has been used to determine currents and or transport properties, such as in relation to surface optical response [10] and electron transport in electron waveguides or through domain walls [12]. The reason for the success of these calculations is that they employed schemes in which the embedding potential was evaluated at the correct energy, ensuring that the derivative of the wavefunction was continuous across S. In practise, there have been few calculations using the non-relativistic embedding scheme in which the energies did not coincide.

There are a number of aspects of the method which are worthy of further consideration. We started with a trial function in which by construction the large component was continuous and the small component discontinuous across the surface S dividing I and II. We could have reversed these conditions, leading to a similar embedded Dirac equation but with a

modified embedding term. The particular choice was motivated by the wish to have a theory which behaves reasonably in the limit $c \longrightarrow \infty$ when the small component becomes negligible—a discontinuous amplitude is not permissible in trial solutions to the Schrödinger equation. However, the behaviour of the alternative formulation should be investigated. Perhaps, in connection with this, there is the question of the spectrum of negative energy solutions, to which we have paid scant attention.

Exploring the $c \longrightarrow \infty$ limit it might be possible to identify how to embed a relativistic region I within a region II treated non-relativistically—a 5d overlayer on a simple metal substrate might be a physical system where such a treatment is appropriate. There could be benefits in terms of computational resources expended if the embedding potential could be determined within the framework of a non-relativistic calculation, and there might also be useful insights in terms of simple models. Finally, in terms of implementation for realistic systems, some of the novel schemes for deriving embedding potentials [3, 5] could certainly be adapted to the relativistic case. It would also be worthwhile to consider whether it is possible to use a restricted electron-like basis, in which the large and small component spinors are combined. This is common practice in most relativistic electronic structure calculations for solids when using basis set techniques (e.g. [17]), and would result in significant computational efficiencies.

References

[1] Inglesfield J E 2000 *J. Phys. C: Solid State Phys.* **14** 3795
[2] Inglesfield J E and Benesh G A 1988 *Phys. Rev.* B **37** 6682
[3] Crampin S, van Hoof J B A N, Nekovee M and Inglesfield J E 1992 *J. Phys.: Condens. Matter* **4** 1475
[4] Benesh G A and Liyanage L S G 1994 *Phys. Rev.* B **49** 17264
   Trioni M, van Hoof J B A N, Crampin S, Brivio G P and Inglesfield J E 1994 *Surf. Sci.* **307–309** 41
   Ishida H 1997 *Surf. Sci.* **388** 71
[5] Ishida H 2001 *Phys. Rev.* B **63** 165409
[6] Nekovee M, Crampin S and Inglesfield J E 1993 *Phys. Rev. Lett.* **70** 3099
   Nekovee M and Inglesfield J E 1992 *Europhys. Lett.* **19** 535
[7] van Hoof J B A N, Crampin S and Inglesfield J E 1992 *J. Phys.: Condens. Matter* **4** 8477
   Li J T, Schneider W-D, Berndt R and Crampin S 1998 *Phys. Rev. Lett.* **80** 3332
[8] Aers G C and Inglesfield J E 1989 *Surf. Sci.* **217** 367
   Clarke S, Inglesfield J E, Nekovee M and de Boer P K 1998 *Phys. Rev. Lett.* **80** 3571
[9] Trioni M I, Brivio G P, Crampin S and Inglesfield J E 1996 *Phys. Rev.* B **53** 8052
   Montalenti F, Trioni M I, Brivio G P and Crampin S 1996 *Surf. Sci.* **364** L595
[10] Ishida H and Liebsch A 1994 *Phys. Rev.* B **50** 4834
   Ishida H, Petukhov A V and Liebsch A 1995 *Surf. Sci.* **340** 1
[11] Ohwaki T, Ishida H and Liebsch A 2003 *Phys. Rev.* B **68** 155422
[12] Dix L and Inglesfield J E 1988 *J. Phys.: Condens. Matter* **10** 5923
   van Hoof J B A N, Schep K M, Brataas A, Bauer G E W and Kelly P J 1999 *Phys. Rev.* B **59** 138
[13] Inglesfield J E 2001 *Comput. Phys. Commun.* **137** 89
[14] Malli G L 1981 *Relativistic Effects in Atoms, Molecules and Solids, NATO ASI Series* vol 87 (New York: Plenum)
[15] MacDonald A H and Vosko S H 1979 *J. Phys. C: Solid State Phys.* **12** 2977
[16] Loucks T 1967 *Augmented Plane Wave Method* (New York: Benjamin)
   Yamagami H 1998 *J. Phys. Soc. Japan* **67** 3176
[17] Theileis V and Bross H 2000 *Phys. Rev.* B **62** 13338
[18] Godreche C 1982 *J. Magn. Magn. Mater.* **29** 262
   Nemoshkalenko V V, Krasovskii A E, Antonov V N, Antonov V N, Fleck U, Wonn H and Zeische P 1983 *Phys. Status Solidi* b **120** 283
   Christensen N E 1984 *Int. J. Quantum Chem.* **25** 233
   Ebert H 1988 *Phys. Rev.* B **38** 9390
[19] Takeda T 1979 *J. Phys. F: Met. Phys.* **9** 815
   Krutzen B C H and Springelkamp F 1989 *J. Phys.: Condens. Matter* **1** 8369

[20] Strange P, Ebert H, Staunton J B and Györffy B L 1989 *J. Phys.: Condens. Matter* **1** 2959
[21] Grass M, Braun J and Borstel G 1994 *Phys. Rev.* B **50** 14827
[22] Strange P, Ebert H, Staunton J B and Györffy B L 1989 *J. Phys.: Condens. Matter* **1** 3947
[23] Ebert H, Battocletti M, Deng M, Freyer H and Voitländer J 1999 *J. Comput. Chem.* **20** 1246
[24] Blaas C, Weinberger P, Szunyogh L, Levy P M and Sommers C B 1999 *Phys. Rev.* B **60** 492
[25] Rotenberg E, Chung J W and Kevan S D 1999 *Phys. Rev. Lett.* **82** 4066
[26] Rose M E 1961 *Relativistic Electron Theory* (New York: Wiley)
     Greiner W 1997 *Relativistic Quantum Mechanics: Wave Equations* (Berlin: Springer)
     Strange P 1998 *Relativistic Quantum Mechanics* (Cambridge: Cambridge University Press)
[27] Stanton R E and Havriliak S 1984 *J. Chem. Phys.* **81** 1910
[28] Abramowitz M and Stegun I A 1965 *Handbook of Mathematical Functions* (New York: Dover)
[29] Halilov S V, Tamura E, Meinert M, Gollisch H and Feder R 1993 *J. Phys.: Condens. Matter* **5** 3859